A new model for binding of kinesin 13 to curved microtubule protofilaments

Anke M. Mulder,[1] Alex Glavis-Bloom,[1] Carolyn A. Moores,[1,2] Michael Wagenbach,[3] Bridget Carragher,[1] Linda Wordeman,[3] and Ronald A. Milligan[1]

[1]Department of Cell Biology, The Scripps Research Institute, La Jolla, CA 92037
[2]School of Crystallography, Birbeck College, University of London, London WC1E 7HX, England, UK
[3]Department of Physiology and Biophysics, University of Washington School of Medicine, Seattle, WA 98104

Kinesin motor proteins use adenosine triphosphate hydrolysis to do work on microtubules (MTs). Most kinesins walk along the MT, but class 13 kinesins instead uniquely recognize MT ends and depolymerize MT protofilaments. We have used electron microscopy (EM) to understand the molecular interactions by which kinesin 13 performs these tasks. Although a construct of only the motor domain of kinesin 13 binds to every heterodimer of a tubulin ring, a construct containing the neck and the motor domain occupies alternate binding sites. Likewise, EM maps of the dimeric full-length (FL) protein exhibit alternate site binding but reveal density for only one of two motor heads. These results indicate that the second head of dimeric kinesin 13 does not have access to adjacent binding sites on the curved protofilament and suggest that the neck alone is sufficient to obstruct access. Additionally, the FL construct promotes increased stacking of rings compared with other constructs. Together, these data suggest a model for kinesin 13 depolymerization in which increased efficiency is achieved by binding of one kinesin 13 molecule to adjacent protofilaments.

Introduction

Microtubules (MTs) are a vital part of the cellular cytoskeleton and are intimately involved in processes such as the transport of molecular cargo, proper chromosome attachment during cell division, and cell structure and morphology (Nogales, 2001; Heald and Nogales, 2002). MTs are dynamic polymers built from heterodimers of α/β-tubulin whose GTP-bound state has a straight conformation that lends itself to polymerization and whose GDP-bound state has a bent conformation that encourages depolymerization of the filament (Desai and Mitchison, 1997). The ability to polymerize and depolymerize in accordance with the localized needs of the cell is an important aspect of MT function and is tightly controlled by a variety of MT-associated proteins (Walczak, 2000). Among these regulators of MT growth and shrinkage are depolymerizing motor proteins such as kinesin 13, which actively depolymerize the MT filament using energy derived from ATP hydrolysis (Walczak et al., 1996; Maney et al., 1998; Desai et al., 1999; Moores et al., 2002).

In contrast to conventional kinesins, which walk along an MT track, kinesin 13s do not walk but instead uniquely recognize MT ends and depolymerize MT protofilaments. It was originally thought that the internal sequence location of the kinesin 13 catalytic domain contributed to its depolymerization activity, as the plus or minus end directionality of other kinesins correlates with N- or C-terminal localizations of the catalytic domain (Vale and Fletterick, 1997; Miki et al., 2001; Lawrence et al., 2004). However, studies have shown that the kinesin 13 catalytic domain alone is sufficient for depolymerization of MT filaments (Moores et al., 2002; Niederstrasser et al., 2002) so that the unique activity of kinesin 13 must be contained within the sequence of its motor core. Structural analysis of the kinesin 13 motor core has revealed that the MT-binding face of the protein has a convex conformation that is strikingly complementary to the surface of a bent protofilament (Ogawa et al., 2004; Shipley et al., 2004), suggesting that depolymerization activity stems, at least in part, from unique interactions between the convex shape of the kinesin 13 motor core and bent tubulin polymer (Ogawa et al., 2004; Shipley et al., 2004). Suggestively, tubulin flexibility is an important stimulator of kinesin 13 ATP

Correspondence to Ronald A. Milligan: milligan@scripps.edu

Abbreviations used in this paper: FL, full length; MCAK, mitotic centromere-associated kinesin; MT, microtubule; NM, neck plus motor core.

The Rockefeller University Press $30.00
J. Cell Biol. Vol. 185 No. 1 51–57
www.jcb.org/cgi/doi/10.1083/jcb.200812052

hydrolysis (Moores and Milligan, 2008), and a recent mutational study indicates that tubulin release precedes ATP turnover (Wagenbach et al., 2008).

Although depolymerization activity is possible with the kinesin 13 motor core alone, the full-length (FL) protein is a more efficient depolymerizer, suggesting important roles for the other domains (Ovechkina et al., 2002; Ogawa et al., 2004; Hertzer et al., 2006). The N terminus of kinesin 13 is important for subcellular localization and contributes to dimerization, whereas the C terminus is required for dimerization (Maney et al., 1998, 2001; Wordeman et al., 1999; Walczak et al., 2002; Kline-Smith and Walczak, 2004). A charged sequence of 60 amino acids N terminal to the catalytic motor domain is a class-specific sequence known as the neck (Ovechkina et al., 2002; Ogawa et al., 2004). The neck is thought to be intimately involved in the depolymerization mechanism, as constructs containing only the neck in addition to the motor domain have depolymerization activity comparable to that seen for FL kinesin 13 (Maney et al., 2001; Ovechkina et al., 2002; Hertzer et al., 2006). The role of the additional N- and C-terminal domains of the FL dimeric protein in the depolymerization mechanism, other than localization and regulation by phosphorylation, is not entirely clear and remains an important line of inquiry.

Structural studies have provided important mechanistic insights into the function of conventional kinesin (e.g., Vale and Milligan, 2000; Endow, 2003), but similar attempts to characterize the interactions of FL kinesin 13 with MT ends have been challenging as a result of their inherent heterogeneity. A recent study has shown that dolastatin-induced tubulin rings mimic the properties of MT ends (flexibility, shape, and stimulation of kinesin 13 ATPase) and that these rings can be decorated with the motor domain of kinesin 13 in various nucleotide states (Moores and Milligan, 2008). The size of these dolastatin tubulin rings and the suggestion that they mimic MT ends make them an ideal system for obtaining structural insights into the depolymerization mechanism of kinesin 13. It is important to note that these dolastatin tubulin rings are synthetic MT end mimics and should not be confused with the bracelets and spirals formed around MTs as products of active depolymerization by mitotic centromere-associated kinesin (MCAK) in the presence of 5′-adenylyl-β,γ-imidodiphosphate (AMPPNP; Moores et al., 2002, 2006; Tan et al., 2006, 2008). Such bracelets are complex and heterogeneous in structure, varying in thickness, connectivity, and symmetry. A beautiful example of careful structural experiments of such bracelets and spirals was recently published (Tan et al., 2008); we believe our experiments with synthetic MT end mimics to be complementary to these important studies.

In this study, we have used EM and single particle image processing methods to visualize the molecular interactions by which kinesin 13 induces depolymerization at MT ends. We have visualized the interactions of kinesin 13 domain constructs of the motor core (M) alone, the neck plus motor core (NM), and the FL protein with MT end mimics in the AMPPNP state. Based on the binding patterns observed in our data, we propose a new model for MT depolymerization in which kinesin 13 achieves increased depolymerization efficiency by binding to adjacent protofilaments.

Results and discussion

Decoration of tubulin rings

As shown in previous studies, incubation of dolastatin-10 with tubulin resulted in the formation of single protofilament rings with 13, 14, and 15× heterodimer geometries, of which rings with the 14× geometry dominated the population (Bai et al., 1999; Boukari et al., 2007; Moores and Milligan, 2008). All kinesin 13 constructs investigated bound these rings along the inner periphery as can be seen by an inner ring of protein density in raw EM micrographs (Fig. 1 A, solid box); this corresponds to the outside MT surface (Bai et al., 1999; Boukari et al., 2007; Moores and Milligan, 2008). Raw EM images show that rings incubated with kinesin 13 constructs assume a less flexible and more rounded shape than undecorated rings (Fig. 1 A, solid vs. dashed box).

A notable difference between ring construct complexes was the presence of stacks of rings in the NM and FL samples (Fig. 1 A, arrows). Such stacks contained tightly associated rings compared with the loosely associated rings occasionally observed for dolastatin rings alone or with the M construct (Fig. 1 A, NM and FL vs. ctrl and M). An inventory of 20 randomly selected micrographs from each of the ring-only, M, NM, and FL AMPPNP datasets confirmed that NM and FL datasets contained more stacks per micrograph than the ring-only and M datasets ($P < 0.001$; Fig. 1 B and see Fig. S3 for equivalent behavior by a human M construct). Notably, stacks formed by FL were 2.41-fold longer than those formed by NM ($P < 0.001$; Fig. 1 C), indicating that dimerization of the motor significantly improved the ability of a single kinesin 13 molecule to interact with multiple rings.

Stack formation in the presence of the monomeric NM construct is likely a result of nonspecific electrostatic interactions between the positively charged neck and the negatively charged tubulin C-terminal tails of nearby rings. Previous studies have suggested multiple roles for such an electrostatic interaction, including that of a motor to substrate tether during depolymerization (Ovechkina et al., 2002; Moores et al., 2006), a weak tether to aid 1D diffusion (Helenius et al., 2006), and an impediment to lateral MT interactions (Ogawa et al., 2004). Aside from providing further support for the existence of such an electrostatic interaction, we do not attribute physiological significance to ring stack formation in the presence of NM. However, because FL forms longer stacks than NM, we hypothesize that in addition to electrostatics, the extra domains present in FL contribute to longer stack formation. As such, these data suggest that the additional N- and C-terminal domains or the second head of dimeric FL is able to bind nearby rings, thereby resulting in the formation of longer stacks of rings.

To further investigate the binding of M, NM, and FL to dolastatin rings, we performed cosedimentation assays of rings incubated with each construct in the presence of AMPPNP and analyzed the results by SDS-PAGE (Fig. 2 A). To compare ring-binding trends between constructs, the molar ratio of construct to heterodimer was determined for each pellet fraction and normalized for the concentration of construct used in the experiment. This analysis revealed that the molar amount of M bound to a

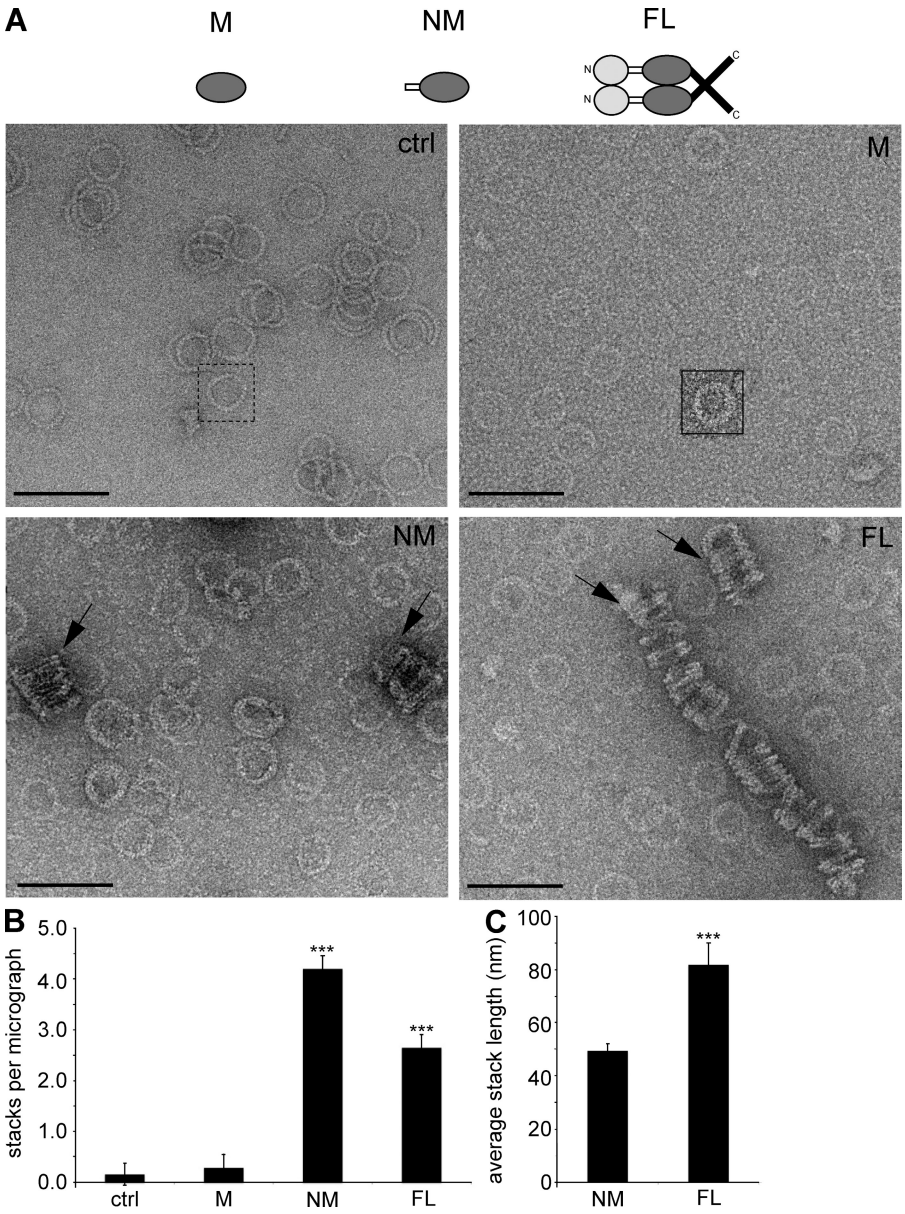

Figure 1. **Decoration of tubulin rings.** (A) Representative images of tubulin rings alone (control [ctrl]) and decorated with the kinesin 13 M, NM, and FL constructs in the presence of AMPPNP. Undecorated rings have flexible shapes (dashed box), whereas decorated rings assume more fixed, rounded shapes (solid box). Arrows mark the stacks that are formed in the presence of NM and FL. The domain organization for each construct is depicted above each micrograph. (B) The mean number of stacks per micrograph was determined for 20 randomly selected micrographs from each dataset. (C) For the NM and FL datasets, the mean length of stacks counted in B was measured. Graphs display mean ± SEM. ***, $P < 0.001$. Bars, 1,000 Å.

given concentration of tubulin rings was 1.28-fold larger than that of NM ($P < 0.05$) and 2.38-fold larger than that of FL ($P < 0.001$), yielding a statistically significant binding trend of M > NM > FL for dolastatin tubulin rings (Fig. 2 B). Significantly, the larger dimeric FL molecule is 1.86-fold less capable of occupying a given number of curved binding sites than NM ($P < 0.01$; Fig. 2 B, NM vs. FL). These data suggest that the additional domains present in FL, and to a lesser extent NM, interfere with the ability of these constructs to occupy binding sites on a curved protofilament.

Single particle image analysis of M, NM, and FL interactions with rings

To gain a better understanding of the structural interactions of kinesin 13 constructs and the curved protofilaments, we used single particle image processing to align and average images of rings and thereby gain increased signal to noise. Such averaging allowed the resolution of individual tubulin monomers, and an arrowhead-shaped protein density bound to tubulin heterodimers along the inner periphery of the ring (Fig. 3 A). Similar to previous observations (Moores and Milligan, 2008), the ring and motor complex revealed handedness, as indicated by the directionality of the tubulin on the outer perimeter and the arrowheaded motor density along the inner perimeter.

Averages of construct ring complexes revealed that NM and FL rarely occupied adjacent sites on the curved protofilament, whereas the M construct consistently occupied every heterodimer-binding site (Fig. 3 A and Fig. S3). Only 4.4% of rings processed in the M dataset passed our cross-correlation threshold for stable alignment to alternate site-binding templates (Fig. S2 and see Materials and methods) compared with 69.4% and 53.9% for the NM and FL datasets. Nonadjacent heterodimer binding was observed for multiple class averages within the NM and FL datasets and support sedimentation assay (Fig. 2) observations that the additional domains in NM and FL interfere with these constructs' abilities to bind curved protofilaments. Furthermore, a dimeric construct lacking the N terminus also showed alternate

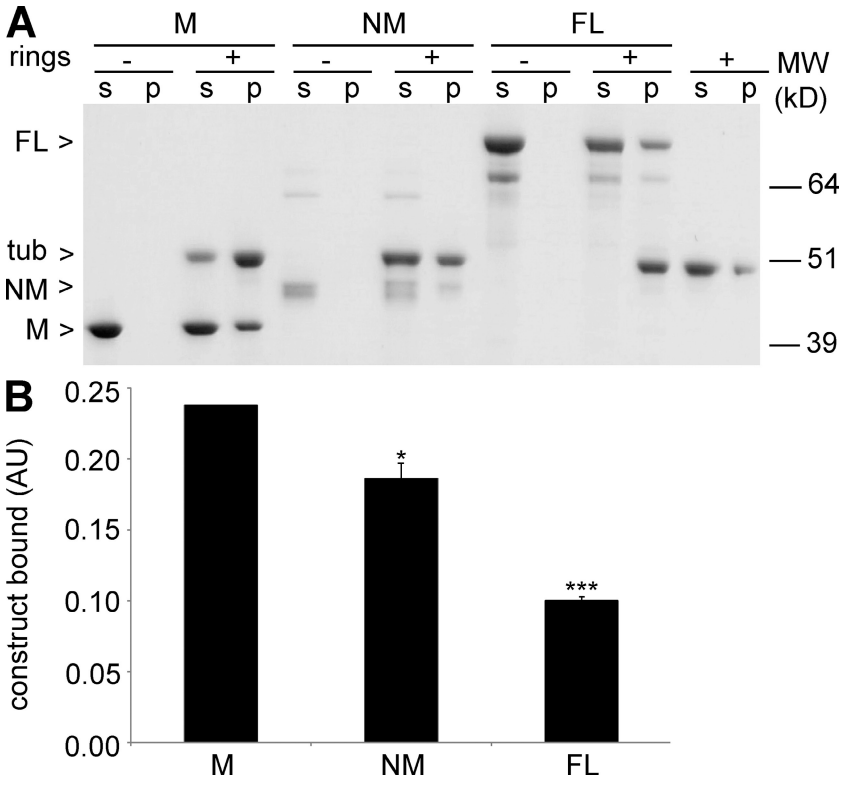

Figure 2. **M, NM, and FL binding to dolastatin rings.** (A) Representative SDS-PAGE gel of sedimentation assays conducted with M, NM, and FL constructs incubated with dolastatin rings in the AMPPNP state. The molar concentrations are 5.1, 3.6, 5.1, and 2.0 µM for M, NM, FL, and heterodimeric tubulin (tub). s, supernatant; p, pellet; MW, molecular weight. (B) OD measurements with a BSA standard curve using ImageJ (Abramoff et al., 2004) software allowed calculation of the motor to heterodimer ratio normalized for starting motor concentration. Values were determined from duplicate experimental runs (not depicted), and repeated sedimentation assays resulted in a binding trend of M > NM > FL for dolastatin rings. Graph displays mean ± SEM. *, $P < 0.05$; ***, $P < 0.001$.

site binding (Fig. S1 C), confirming that dimeric kinesin 13 is precluded from adjacent site binding on the curved protofilament and suggesting that the N terminus is not involved in the preclusion of adjacent site binding. These observations, together with stack formation data (Fig. 1), suggest that FL would rather bind nearby protofilaments than occupy adjacent binding sites on a single curved protofilament.

Interaction of M, NM, and FL with bent α/β-tubulin heterodimer

To locate the additional domains present in the FL and NM constructs and better understand their contribution to alternate site binding, we computationally cut out individual motor–heterodimer complexes from the 14-mer ring class averages and analyzed these particles by single particle averaging methods (Fig. 3 B). Visual comparison of motor–heterodimer averages revealed key differences in the appearance of the M, NM, and FL motor densities. The M construct assumed a compact conformation on the heterodimer compared with more extended conformations assumed by the NM and FL constructs (Fig. 3 B, M vs. NM and FL). The NM and FL constructs had the characteristic arrowhead shape that has been previously observed for MCAK (Ogawa et al., 2004; Shipley et al., 2004). The larger FL construct revealed some diffuse density to either side of the motor core (Fig. 3 B, FL), likely as a result of conformational heterogeneity in its additional N- and C-terminal domains.

Difference map comparisons between motor–heterodimer averages of M, NM, and FL confirmed the statistically significant absence of motors to either side of the NM and FL cores (Fig. 3 B, arrowheads, $P < 0.01$), a feature that was notably absent in the FL-NM difference map (Fig. 3 B, bottom). Additionally, FL-M and FL-NM difference maps did not visualize a density attributable to the second polypeptide of the dimeric FL construct (Fig. 3 B, middle and bottom), suggesting that it does not assume a fixed position on the ring and that this density was lost during averaging of multiple images. These results support our findings that NM and FL engage in alternate site binding on the curved protofilament and that the two heads of dimeric FL are not engaged on the same ring.

Importantly, NM-M and FL-M difference maps revealed additional density to the minus end side of the NM and FL motor cores (Fig. 3 B, arrows, $P < 0.01$), a feature that was absent in the FL-NM difference map (Fig. 3 B, bottom). The additional density in the NM and FL averages was observed for motor–heterodimers excised from multiple class averages and was not observed within construct datasets. That this density was observed in both the FL-M and NM-M difference maps but not in the FL-NM difference map suggests that the extended conformations of FL and NM as compared with M are at least in part attributable to the neck domain.

Models of a kinesin 13 NM crystal structure fitted onto straight and bent protofilaments reveal significant steric hindrance to adjacent site binding on the curved protofilament (Fig. 3 B, top vs. bottom; Nogales et al., 1999; Ogawa et al., 2004; Ravelli et al., 2004). The NM crystal structure indicates that such steric hindrance could be caused by the neck domain alone (Fig. 3 C, red domain) or through interaction of the neck with the L2 loop. Notably, a second crystal structure of NM (Ogawa et al., 2004) has a more compact conformation in which the neck domain points toward the adjacent protofilament (Fig. 3 C, red arrow); such a conformation of NM could potentially accommodate adjacent site binding on the curved protofilament. Indeed, a recent structure of bracelet rings induced by M from *Drosophila melanogaster*

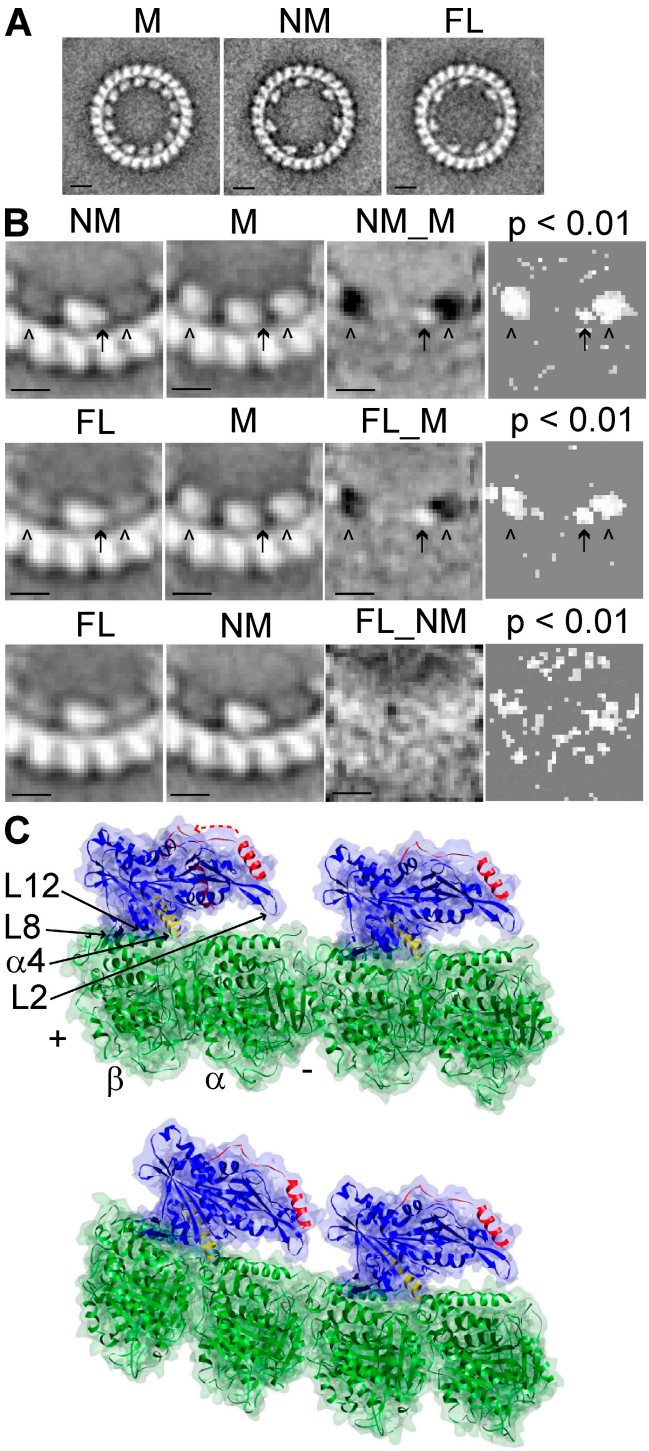

Figure 3. **Kinesin 13 neck obstructs adjacent binding-site access on curved α/β-heterodimers.** (A) Representative class averages for dolastatin rings decorated with M, NM, and FL. Bars, 100 Å. (B) Representative class averages (M, NM, and FL), difference maps (NM-M, FL-M, and FL-NM), and Student's *t* test maps (right column) for motor–heterodimer cutouts. Arrowheads mark the adjacent binding site on the curved protofilament, and arrows mark the position of extra density seen in NM and FL. Bars, 50 Å. (C) Model of the crystal structures of truncated NM (Protein Data Bank reference codes 2HEH and 1v8k) fitted onto straight (Protein Data Bank reference code 1tub) and bent tubulin (Protein Data Bank reference code 1sa0). The region in red corresponds to the neck domain, the red arrow indicates the difference in neck orientation between the two crystal structures, the region in yellow indicates the α-relay helix, and other important domains are marked.

kinesin 13 accommodates the compact structure of NM in adjacent M densities along a curved protofilament (Tan et al., 2008).

Further examination of the fitted crystal structures (Fig. 3 C) show that the C terminus of NM extends parallel to the α-4 relay helix (Fig. 3 C, yellow) toward adjacent protofilaments. Extension along this axis of the C-terminal coiled coil of FL kinesin 13 could prime the motor for dimerization in a manner that allows adjacent protofilament access. Significantly, because kinesin 13 dimerizes through both its N and C termini (Maney et al., 2001) and the N terminus would extend from the neck domain, the motor would be locked on both ends in a conformation with better access to adjacent protofilaments than to adjacent sites on the same protofilament.

Model for interaction of kinesin 13 with curved protofilaments

The monomeric NM construct has reduced ability to bind curved protofilaments (Figs. 2 and 3), suggesting that the neck domain alone is sufficient to preclude adjacent site access; however, NM-induced stack formation (Fig. 1) would argue that this domain interacts with adjacent protofilaments as well as precluding access to binding sites on a single protofilament. Previous studies have reported that the NM construct exists in an extended and compact state (Ems-McClung et al., 2007), and the existence of two different NM x-ray structures (Fig. 3 C) confirms the flexibility of this domain (Ogawa et al., 2004). Importantly, there is precedent for regulation of the neck by the N terminus (Ems-McClung et al., 2007), and our observations that a construct consisting of the N terminus in addition to NM assumes a more compact conformation on dolastatin rings (Fig. S1 C) support this idea. Together with our results, these observations suggest that the neck domain of NM can assume an extended conformation that precludes (Fig. 4 A, top) and a compact conformation that accommodates (Fig. 4 A, bottom) adjacent site binding on curved protofilaments. Our modeling experiments indicate that both conformations of NM should decorate adjacent binding sites on straight protofilaments (Fig. 3 C and Fig. 4 A).

The observations that FL has a reduced ability to decorate curved protofilaments (Figs. 2 and 3) suggest that this construct is sterically hindered from adjacent site binding. The absence of well-resolved densities for the N and C termini or the second polypeptide of FL in EM averages (Fig. 3, A and B) indicates that these domains are flexible. Extensive conformational variability has been previously reported for FL (Ems-McClung et al., 2007). Together with ring stack formation by FL (Fig. 1), these observations suggest that the second polypeptide of dimeric FL is available for binding to adjacent protofilaments. We propose that the design and size of FL precludes adjacent site binding on straight and curved protofilaments so that this dimeric motor preferentially binds adjacent protofilaments on the MT lattice (Fig. 4 B). Such a configuration of binding by FL would allow increased depolymerization efficiency by enabling the dimeric motor to depolymerize two protofilaments at the same time.

An intriguing alternative interpretation of nonadjacent binding by FL is one in which motor densities on nonadjacent heterodimers belong to a single dimeric FL molecule. This might be suggestive of a depolymerization mechanism that combines

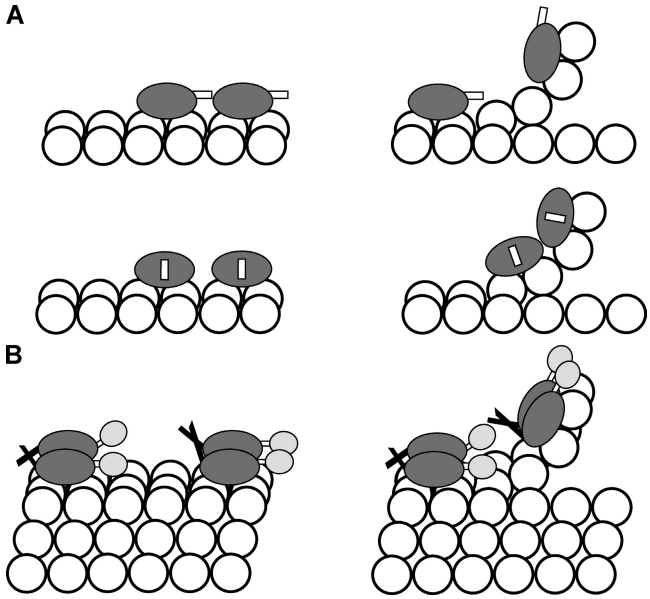

Figure 4. **Model for MT depolymerization by kinesin 13.** (A) The NM construct can assume an extended (top) or compact (bottom) conformation. These correspond to the crystal structures (Protein Data Bank reference codes 2HEH and 1v8k) shown in Fig. 3 B. Both conformations can decorate adjacent binding sites on straight protofilaments (left), but the extended conformation decorates alternate binding sites on a curved protofilament (top right). (B) The dimeric FL construct is designed to bind two adjacent protofilaments instead of binding adjacent heterodimers on a single protofilament. Because of its size and design, this motor is postulated to bind alternate binding sites on both straight and curved protofilaments, although our data only provide evidence for the latter.

alternate site binding with processivity to separate terminal tubulin from a curling protofilament via steric strain. However, our observations that both NM and FL engage in alternate site binding and that FL forms longer stacks than NM seem to argue against this possibility. A further potential concern with the proposed model is that staggered FL dimers could stabilize (as opposed to destabilize) the MT end via intraprotofilament cross-bridging. We believe this to be an unlikely scenario for the following reasons: (a) the alternate site-binding requirement guarantees that the terminal two heterodimers of every pair of protofilaments are free to peel away from its neighbors even with cross-linking of multiple kinesin 13s, (b) high and low affinity kinesin 13–binding cycles in the presence of ATP reduce the probability of saturating the MT end with staggered kinesin 13s, and (c) intraprotofilament cross-linking would not inhibit kinesin 13 activity, so this scenario is more likely to result in multiprotofilament depolymerization products than to prevent depolymerization altogether.

The model presented in this study represents a divergence from the processivity along a single protofilament observed for conventional kinesin. As such, it is vital to extend and validate these observations in the context of MTs; such experiments are ongoing in our laboratory.

Materials and methods

Protein expression and purification

Constructs were prepared as described previously: M is from *Plasmodium falciparum* (Moores et al., 2002) and represents the kinesin 13 catalytic motor core. NM includes residues 182–583 of kinesin 13 from *Cricetulus griseus* (Ovechkina et al., 2002). FL (also known as Q710) contains all but the last eight residues of kinesin 13 from *C. griseus* (Moore and Wordeman, 2004). ΔN (residues 182–718) and ΔC (residues 1–583) are N- and C-terminal deletions of *C. griseus* MCAK, prepared similar to FL. M, NM, and ΔC exist as monomers in solution, whereas FL and ΔN exist as dimers (Hertzer et al., 2006; Ems-McClung et al., 2007). The use of M from *P. falciparum* was necessitated by the fact that M from *C. griseus* was incurably prone to aggregation, which prevented us from performing experiments with it (our unpublished observations). However, using a human MCAK M construct (88% sequence identity with *C. griseus* MCAK) with MT depolymerization activity, we observed adjacent site binding to, and degree of stack formation of, dolastatin rings in a manner indistinguishable from the *P. falciparum* M construct (Fig. S3). Thus, the phenomena that we describe are unlikely to be a result of species-specific properties of our constructs but instead relate to a generalized mechanism for kinesin 13 MT depolymerization. The human M construct (residues 257–593) was provided by Cytokinetics.

Kinesin 13 and ring complex formation

Rings were formed by incubating 0.04 mM dolastatin-10 dissolved in DMSO with 2 mg/ml GTP-tubulin (Cytoskeleton, Inc.) in 40 mM Pipes, pH 6.8, 1.50 mM $MgCl_2$, and 12% (vol/vol) DMSO for 20 min at room temperature. Kinesin 13 constructs were dialyzed into BrB80-KCl buffer (80 mM Pipes, pH 6.8, 2 mM $MgCl_2$, 1 mM EGTA, and 100 mM KCl) at 4°C stirring for 3–4 h. Constructs were mixed with 5 mM AMPPNP and 0.5 µM rings in BrB80-KCl at 3 µM for 2–3 min at room temperature. Sedimentation assay reaction mixtures were ultracentrifuged in a rotor (TLA-100; Beckman Coulter) at 100,000 rpm at room temperature for 20 min. The supernatant and pellet were separated, subjected to SDS-PAGE analysis, and the amount of protein in each lane was estimated using ImageJ (National Institutes of Health; Abramoff et al., 2004) and a BSA standard curve.

EM sample preparation and data collection

EM samples were prepared on 400-mesh copper continuous carbon grids that were cleaned using a plasma cleaner (5 s; 25% O_2 and 75% Ar; Solarus) immediately before use. A 5-µl drop of sample was applied to the grid, washed with BrB80-KCl, and negatively stained with 1% uranyl acetate. EM was performed at room temperature using a transmission electron microscope (Tecnai F20; FEI) at 120 kiloelectronvolts (keV) with a 4,000 × 4,000 charge-coupled device camera (Gatan), and data were collected in low dose at −2 µm defocus at 50,000× magnification using Leginon (Suloway et al., 2005) in manual mode.

Image processing

Image processing was done in SPIDER (Frank et al., 1996) with functions available from Appion (Lander et al., 2009). In Appion, micrograph quality was assessed, particles were picked and boxed, and initial reference-free alignment and classification was performed on ∼2,000 rings for each dataset. Classes with well-stained particles underwent reference-based alignment in SPIDER to sort out 13-, 14-, and 15-mer rings. Only 14-mer rings (∼80% of all particles) were processed further. Particles underwent reference-based alignment, correspondence analysis, and hierarchical ascendant classification in SPIDER to sort out alternate binding rings (Fig. S2; Frank et al., 1996). Particles were considered alternate binders for cross-correlation coefficients ≥1,800, resulting in ∼20%, ∼80%, and ∼80% alternate binders for M, NM, and FL, respectively. Particles that did not reach stable alignment or failed to pass visual inspection were thrown out, resulting in 4.4, 69.4, and 53.9% alternate binders for M, NM, and FL datasets. Individual motor–tubulin complexes were picked manually in the EMAN Boxer program (Ludtke et al., 1999) from alternate binding class averages. These particles underwent two rounds of reference-based alignment and classification in SPIDER (Frank et al., 1996). Difference maps and Student's *t* tests were calculated in SPIDER (Frank et al., 1996) and Phoelix (Whittaker et al., 1995).

Fitting kinesin 13 crystal structure into tubulin rings

Chimera 1.2470 (Pettersen et al., 2004) was used for all fitting experiments. An EM density map of Ncd (nonclaret disjunctional kinase-like protein)-MT (Endres et al., 2006) was the scaffold for fitting α- and β-tubulin (Nogales et al., 1998) and Ncd (Sablin et al., 1998) crystal structures using the "fit model into map" feature. The two crystal structures of truncated NM, KIF2C (Ogawa et al., 2004), were fitted using the "matchmaker" feature until all atoms agreed within 0.345 Å. To model the interaction with a curved protofilament, the fitted model of KIF2C and straight β-tubulin were used as a scaffold for fitting a crystal structure of stathmin-bound tubulin dimers (Ravelli et al., 2004) until all atoms of β-tubulin agreed within 0.345 Å. As our experimental data did not yield 3D density information, we did not use our 2D

EM projection maps to constrain these 3D models; however, we were pleased to note that a recent EM map of the *Drosophila* M construct bound to protofilament bracelets supports our model for kinesin 13 M domain interactions with a curved substrate (Tan et al., 2008).

Online supplemental material

Fig. S1 shows eigenimages and additional class averages, Fig. S2 shows derivation of alternate site-binding templates, and Fig. S3 shows EM analysis of M construct from human MCAK. Online supplemental material is available at http://www.jcb.org/cgi/content/full/jcb.200812052/DC1.

We thank Craig Yoshioka, Elizabeth Wilson-Kubalek, Matthew Lee, Crystal Moran, and members of the Milligan and the Automated Molecular Imaging groups (The Scripps Research Institute, La Jolla, CA) for helpful discussions and Steve Bradlow and Henry Bradlow for mathematical assistance.

This work was supported by grants from the National Institutes of Health (GM52468 to R.A. Milligan and GM69429 to L. Wordeman) and the National Science Foundation (Predoctoral Fellowship to A.M. Mulder). Some of the work was conducted at the National Resource for Automated Molecular Microscopy, which is supported by the National Institutes of Health (grant RR175173).

Submitted: 9 December 2008
Accepted: 10 March 2009

References

Abramoff, M.D., P.J. Magelhaes, and S.J. Ram. 2004. Image processing with ImageJ. *Biophotonics International.* 11:36–42.

Bai, R., N.A. Durso, D.L. Sackett, and E. Hamel. 1999. Interactions of the sponge-derived antimitotic tripeptide hemiasterlin with tubulin: comparison with dolastatin 10 and cryptophycin 1. *Biochemistry.* 38:14302–14310.

Boukari, H., D.L. Sackett, P. Schuck, and R.J. Nossal. 2007. Single-walled tubulin ring polymers. *Biopolymers.* 86:424–436.

Desai, A., and T.J. Mitchison. 1997. Microtubule polymerization dynamics. *Annu. Rev. Cell Dev. Biol.* 13:83–117.

Desai, A., S. Verma, T.J. Mitchison, and C.E. Walczak. 1999. Kin I kinesins are microtubule-destabilizing enzymes. *Cell.* 96:69–78.

Ems-McClung, S.C., K.M. Hertzer, X. Zhang, M.W. Miller, and C.E. Walczak. 2007. The interplay of the N- and C-terminal domains of MCAK control microtubule depolymerization activity and spindle assembly. *Mol. Biol. Cell.* 18:282–294.

Endow, S.A.. 2003. Kinesin motors as molecular machines. *Bioessays.* 25:1212–1219.

Endres, N.F., C. Yoshioka, R.A. Milligan, and R.D. Vale. 2006. A lever-arm rotation drives motility of the minus-end-directed kinesin Ncd. *Nature.* 439:875–878.

Frank, J., M. Radermacher, P. Penczek, J. Zhu, Y. Li, M. Ladjadj, and A. Leith. 1996. SPIDER and WEB: processing and visualization of images in 3D electron microscopy and related fields. *J. Struct. Biol.* 116:190–199.

Heald, R., and E. Nogales. 2002. Microtubule dynamics. *J. Cell Sci.* 115:3–4.

Helenius, J., G. Brouhard, Y. Kalaidzidis, S. Diez, and J. Howard. 2006. The depolymerizing kinesin MCAK uses lattice diffusion to rapidly target microtubule ends. *Nature.* 441:115–119.

Hertzer, K.M., S.C. Ems-McClung, S.L. Kline-Smith, T.G. Lipkin, S.P. Gilbert, and C.E. Walczak. 2006. Full-length dimeric MCAK is a more efficient microtubule depolymerase than minimal domain monomeric MCAK. *Mol. Biol. Cell.* 17:700–710.

Kline-Smith, S.L., and C.E. Walczak. 2004. Mitotic spindle assembly and chromosome segregation: refocusing on microtubule dynamics. *Mol. Cell.* 15:317–327.

Lander, G.C., S.M. Stagg, N.R. Voss, A. Cheng, D. Fellmann, J. Pulokas, C. Yoshioka, C. Irving, A. Mulder, P.W. Lau, et al. 2009. Appion: an integrated, database-driven pipeline to facilitate EM image processing. *J. Struct. Biol.* 166:95–102.

Lawrence, C.J., R.K. Dawe, K.R. Christie, D.W. Cleveland, S.C. Dawson, S.A. Endow, L.S. Goldstein, H.V. Goodson, N. Hirokawa, J. Howard, et al. 2004. A standardized kinesin nomenclature. *J. Cell Biol.* 167:19–22.

Ludtke, S.J., P.R. Baldwin, and W. Chiu. 1999. EMAN: semiautomated software for high-resolution single-particle reconstructions. *J. Struct. Biol.* 128:82–97.

Maney, T., A.W. Hunter, M. Wagenbach, and L. Wordeman. 1998. Mitotic centromere-associated kinesin is important for anaphase chromosome segregation. *J. Cell Biol.* 142:787–801.

Maney, T., M. Wagenbach, and L. Wordeman. 2001. Molecular dissection of the microtubule depolymerizing activity of mitotic centromere-associated kinesin. *J. Biol. Chem.* 276:34753–34758.

Miki, H., M. Setou, K. Kaneshiro, and N. Hirokawa. 2001. All kinesin superfamily protein, KIF, genes in mouse and human. *Proc. Natl. Acad. Sci. USA.* 98:7004–7011.

Moore, A., and L. Wordeman. 2004. C-terminus of mitotic centromere-associated kinesin (MCAK) inhibits its lattice-stimulated ATPase activity. *Biochem. J.* 383:227–235.

Moores, C.A., and R.A. Milligan. 2008. Visualisation of a kinesin-13 motor on microtubule end mimics. *J. Mol. Biol.* 377:647–654.

Moores, C.A., M. Yu, J. Guo, C. Beraud, R. Sakowicz, and R.A. Milligan. 2002. A mechanism for microtubule depolymerization by KinI kinesins. *Mol. Cell.* 9:903–909.

Moores, C.A., J. Cooper, M. Wagenbach, Y. Ovechkina, L. Wordeman, and R.A. Milligan. 2006. The role of the kinesin-13 neck in microtubule depolymerization. *Cell Cycle.* 5:1812–1815.

Niederstrasser, H., H. Salehi-Had, E.C. Gan, C. Walczak, and E. Nogales. 2002. XKCM1 acts on a single protofilament and requires the C terminus of tubulin. *J. Mol. Biol.* 316:817–828.

Nogales, E. 2001. Structural insight into microtubule function. *Annu. Rev. Biophys. Biomol. Struct.* 30:397–420.

Nogales, E., S.G. Wolf, and K.H. Downing. 1998. Structure of the alpha beta tubulin dimer by electron crystallography. *Nature.* 391:199–203.

Nogales, E., M. Whittaker, R.A. Milligan, and K.H. Downing. 1999. High-resolution model of the microtubule. *Cell.* 96:79–88.

Ogawa, T., R. Nitta, Y. Okada, and N. Hirokawa. 2004. A common mechanism for microtubule destabilizers-M type kinesins stabilize curling of the protofilament using the class-specific neck and loops. *Cell.* 116:591–602.

Ovechkina, Y., M. Wagenbach, and L. Wordeman. 2002. K-loop insertion restores microtubule depolymerizing activity of a "neckless" MCAK mutant. *J. Cell Biol.* 159:557–562.

Pettersen, E.F., T.D. Goddard, C.C. Huang, G.S. Couch, D.M. Greenblatt, E.C. Meng, and T.E. Ferrin. 2004. UCSF Chimera–a visualization system for exploratory research and analysis. *J. Comput. Chem.* 25:1605–1612.

Ravelli, R.B., B. Gigant, P.A. Curmi, I. Jourdain, S. Lachkar, A. Sobel, and M. Knossow. 2004. Insight into tubulin regulation from a complex with colchicine and a stathmin-like domain. *Nature.* 428:198–202.

Sablin, E.P., R.B. Case, S.C. Dai, C.L. Hart, A. Ruby, R.D. Vale, and R.J. Fletterick. 1998. Direction determination in the minus-end-directed kinesin motor ncd. *Nature.* 395:813–816.

Shipley, K., M. Hekmat-Nejad, J. Turner, C. Moores, R. Anderson, R. Milligan, R. Sakowicz, and R. Fletterick. 2004. Structure of a kinesin microtubule depolymerization machine. *EMBO J.* 23:1422–1432.

Suloway, C., J. Pulokas, D. Fellmann, A. Cheng, F. Guerra, J. Quispe, S. Stagg, C.S. Potter, and B. Carragher. 2005. Automated molecular microscopy: the new Leginon system. *J. Struct. Biol.* 151:41–60.

Tan, D., A.B. Asenjo, V. Mennella, D.J. Sharp, and H. Sosa. 2006. Kinesin-13s form rings around microtubules. *J. Cell Biol.* 175:25–31.

Tan, D., W.J. Rice, and H. Sosa. 2008. Structure of the kinesin13-microtubule ring complex. *Structure.* 16:1732–1739.

Vale, R.D., and R.J. Fletterick. 1997. The design plan of kinesin motors. *Annu. Rev. Cell Dev. Biol.* 13:745–777.

Vale, R.D., and R.A. Milligan. 2000. The way things move: looking under the hood of molecular motor proteins. *Science.* 288:88–95.

Wagenbach, M., S. Domnitz, L. Wordeman, and J. Cooper. 2008. A kinesin-13 mutant catalytically depolymerizes microtubules in ADP. *J. Cell Biol.* 183:617–623.

Walczak, C.E. 2000. Microtubule dynamics and tubulin interacting proteins. *Curr. Opin. Cell Biol.* 12:52–56.

Walczak, C.E., T.J. Mitchison, and A. Desai. 1996. XKCM1: a *Xenopus* kinesin-related protein that regulates microtubule dynamics during mitotic spindle assembly. *Cell.* 84:37–47.

Walczak, C.E., E.C. Gan, A. Desai, T.J. Mitchison, and S.L. Kline-Smith. 2002. The microtubule-destabilizing kinesin XKCM1 is required for chromosome positioning during spindle assembly. *Curr. Biol.* 12:1885–1889.

Whittaker, M., B.O. Carragher, and R.A. Milligan. 1995. PHOELIX: a package for semi-automated helical reconstruction. *Ultramicroscopy.* 58:245–259.

Wordeman, L., M. Wagenbach, and T. Maney. 1999. Mutations in the ATP-binding domain affect the subcellular distribution of mitotic centromere-associated kinesin (MCAK). *Cell Biol. Int.* 23:275–286.